miR-582-5p targets Skp1 and regulates NF-κB signaling-mediated inflammation

李, 栄智

Archives of Biochemistry and Biophysics 734 (2023) 109501

Contents lists available at ScienceDirect

Archives of Biochemistry and Biophysics

journal homepage: www.elsevier.com/locate/yabbi

miR-582-5p targets *Skp1* and regulates NF-κB signaling-mediated inflammation

Rongzhi Li [a], Tomomi Sano [b,*], Akiko Mizokami [c], Takao Fukuda [a], Takanori Shinjo [a], Misaki Iwashita [a], Akiko Yamashita [a], Terukazu Sanui [a], Yusuke Nakatsu [d], Yusuke Sotomaru [e], Tomoichiro Asano [d], Takashi Kanematsu [b], Fusanori Nishimura [a]

[a] Department of Periodontology, Division of Oral Rehabilitation, Faculty of Dental Science, Kyushu University, Fukuoka, Japan
[b] Department of Cell Biology, Aging Science, and Pharmacology, Division of Oral Biological Sciences, Faculty of Dental Science, Kyushu University, Fukuoka, Japan
[c] Oral, Brain and Total Health Science, Faculty of Dental Science, Kyushu University, Fukuoka, Japan
[d] Department of Biological Chemistry, Institute of Biomedical and Health Sciences, Hiroshima University, Hiroshima, Japan
[e] Natural Science Center for Basic Research and Development, Hiroshima University, Hiroshima, Japan

ARTICLE INFO

Handling Editor: Dr H Forman

Keywords:
Inflammation
microRNA
miR-582-5p
NF-κB signaling
SKP1

ABSTRACT

A well-tuned inflammatory response is crucial for an effective immune process. Nuclear factor-kappa B (NF-κB) is a key mediator of inflammatory and innate immunity responses, and its dysregulation is closely associated with immune-related diseases. MicroRNAs (miRNAs) are important inflammation modulators. However, miRNA-regulated mechanisms that implicate NF-κB activity are not fully understood. This study aimed to identify a potential miRNA that could modulate the dysregulated NF-κB signaling during inflammation. We identified miR-582-5p that was significantly downregulated in inflamed murine adipose tissues and RAW264.7 cells. S-phase kinase-associated protein 1 (SKP1), a core component of an E3 ubiquitin ligase that regulates the NF-κB pathway, was proposed as a biological target of miR-582-5p by using TargetScan. The binding of miR-582-5p to a 3′-untranslated region site on *Skp1* was confirmed using a dual-luciferase reporter assay; in addition, transfection with a miR-582-5p mimic suppressed SKP1 expression in RAW264.7 cells. Importantly, exogenous miR-582-5p attenuated the production of pro-inflammatory cytokines such as tumor necrosis factor-alpha, interleukin-1 beta, and interleukin-6 through suppressing the degradation of the NF-κB inhibitor alpha, followed by the nuclear translocation of NF-κB. Therefore, exogenously applied miR-582-5p can attenuate the NF-κB signaling pathway *via* targeting *Skp1*; this provides a prospective therapeutic strategy for treating inflammatory and immune diseases.

1. Introduction

Inflammation is a protective response against harmful stimuli. A well-orchestrated inflammatory process is crucial for maintaining homeostasis. However, a dysregulated and prolonged inflammatory response is responsible for the pathogenesis of various diseases, such as obesity [1–3].

Macrophages play important roles in inflammation through the production of inflammatory cytokines such as tumor necrosis factor-α (TNF-α) [4]. Pattern recognition receptor (PRR), which recognizes pathogen-associated molecular patterns, activates macrophages. The PRR Toll-like receptor 4 (TLR4) senses the gram-negative bacterial outer membrane component lipopolysaccharide (LPS) and initiates the myeloid differentiation primary response gene 88 (MyD88)-dependent nuclear factor-kappa B (NF-κB) pathway [5]. NF-κB signaling is a prototypical pro-inflammatory signaling pathway regulating the expression of a wide range of genes associated with immune and inflammation responses [1,6,7]. Dysregulation of NF-κB signaling causes various diseases, including obesity. In obese adipose tissue, the activation of NF-κB signaling in accumulated macrophages upregulates the expression of several pro-inflammatory genes such as TNF-α, interleukin-1β (IL-1β), and interleukin-6 (IL-6); this promotes a chronic systemic low-grade inflammation [8], thereby suppressing insulin action. Thus, obese adipose tissue provides a suitable model for the investigation of NF-κB dysregulation. Therefore, identifying the novel molecular mechanism regulating the NF-κB signaling pathway is important for treating inflammation-associated diseases.

* Corresponding author.
E-mail address: tomoming@dent.kyushu-u.ac.jp (T. Sano).

https://doi.org/10.1016/j.abb.2022.109501
Received 11 September 2022; Received in revised form 15 December 2022; Accepted 30 December 2022
Available online 31 December 2022

Abbreviations

3′-UTR	3′-untranslated region
βTrCP	beta transducin repeat-containing protein
CUL1	cullin 1
DMEM	Dulbecco's modified Eagle medium
ELISA	enzyme-linked immunosorbent assay
eWAT	epididymal white adipose tissue
GAPDH	glyceraldehyde-3-phosphate dehydrogenase
HFD	high fat diet;
IκBα	nuclear factor of kappa light polypeptide gene enhancer in B-cells inhibitor, alpha
IL-1β	interleukin-1 beta
IL-6	interleukin-6
LPS	lipopolysaccharide;
MAF	mature adipocytes fraction
miRNA	microRNA
mRNA	messenger RNA
MyD88	myeloid differentiation primary response gene 88
NC-miR mimic	negative control microRNA mimic
ND	normal diet;
NF-κB	nuclear factor-kappa B
PBS	phosphate-buffered saline;
PRR	pattern recognition receptor
qPCR	quantitative PCR
Rbx1	ring-box 1
SCF	SKP1-CUL1-F-box protein
siRNA	small interfering RNA
SKP1	S-phase kinase-associated protein 1
SVF	stromal vascular fraction
TLR	Toll-like receptor
TNF-α	tumor necrosis factor-alpha

In resting cells, the NF-κB heterodimer p65/p50 binds to the NF-κB inhibitor alpha (IκBα) and remains inactive in the cytoplasm. Upon stimulation, signal transduction activates the IκB kinase complex to phosphorylate IκBα. Phosphorylated IκBα is polyubiquitinated by an E3 ubiquitin ligase, and the polyubiquitinated IκBα is subsequently degraded by the 26S proteasome [9]. This polyubiquitination process is regulated by S-phase kinase-associated protein 1 (SKP1) - cullin 1 (CUL1) - F-box protein (SCF E3 ligase complex) [10]. IκB kinase phosphorylates p65, and the NF-κB heterodimer p65/p50 is rapidly translocated into the nucleus, where it upregulates the transcription of target genes such as TNF-α, IL-1β, and IL-6 [9,11].

MicroRNAs (miRNAs) are endogenous small non-coding RNAs (20–24 nucleotides) that are highly conserved through evolution [12]. miRNAs post-transcriptionally regulate protein expression through complementary binding to the 3′-untranslated region (3′-UTR) of its target messenger RNA (mRNA). miRNAs play important regulatory roles in many biological processes and contribute to various pathologies, including inflammatory diseases, metabolic disorders, and tumors [12–14]. miRNAs are closely associated with NF-κB signaling [15]. miR-146a-5p attenuates liver fibrogenesis [16] and inflammation [17,18] by suppressing the expression of interleukin-1 receptor-associated kinase 1 and TNF receptor-associated factor 6, which function in LPS-stimulated NF-κB pathway. miR-27a blocks the activation of NF-κB signaling by targeting the TLR4 gene [19].

In this study, we identified a novel miRNA, miR-582-5p, which is downregulated in inflamed macrophages and regulates NF-κB signaling during inflammation. Transfection of RAW264.7 cells, murine macrophage cells, with the miR-582-5p mimic attenuated LPS-induced activation of NF-κB signaling followed by cytokine production by targeting the *Skp1* gene. This novel miRNA is a therapeutic target for treating NF-κB signaling-mediated inflammation.

2. Materials and methods

2.1. Mice

Eight-week-old male C57BL/6J mice were obtained from the Natural Science Center for Basic Research and Development of Hiroshima University. Mice were randomized into experimental groups and fed either a normal diet with 5% fat (ND, Oriental Yeast Co., Tokyo, Japan) or a 60% kcal high-fat diet (HFD, Oriental Yeast Co.) *ad libitum* for eight weeks. Changes in body weight and food intake were monitored as described previously [20]; the mice were sacrificed at 16 weeks of age.

All procedures were approved by the Institutional Animal Care and Use Committee of Hiroshima University (permission number: A22-65), and the animals were maintained following the Guide for Hiroshima University Animal Experimentation Regulation.

2.2. Cell culture and stimulation

The murine macrophage cell line, RAW264.7, was obtained from American Type Culture Collection (ATCC, Manassas, VA, USA). The cells were cultured in Dulbecco's modified Eagle medium (DMEM, Nacalai Tesque, Kyoto, Japan) supplemented with 10% fetal bovine serum (FBS, Sigma Aldrich, Saint Louis, MO, USA) and 1% penicillin-streptomycin (Nacalai Tesque), as described earlier [21]. The cells were cultured in an incubator at 37 °C in a humidified 5% CO_2 atmosphere.

Murine 3T3-L1 preadipocytes (ATCC) were cultured in DMEM containing 10% FBS and 1% penicillin-streptomycin. The differentiation procedure of 3T3-L1 cells was performed as previously described [18]. Briefly, once the 3T3-L1 fibroblasts reached confluence, differentiation was induced with 4 μg/mL dexamethasone (Sigma Aldrich), 0.5 mM 3-isobutyl-1-methylxanthine (Sigma Aldrich), and 200 nM insulin (Cell Science & Technology Institute, Sendai, Japan). At 48 h after the induction of differentiation, the medium was replaced with DMEM containing 10% FBS and 1 μM insulin every 2–3 days until the harvest of the cells.

Mouse bone marrow cells were isolated from femurs and tibiae of six-week-old male C57BL/6J mice and differentiated into bone marrow-derived macrophages in an α-minimal essential medium (Nacalai Tesque) supplemented with 50 ng/mL macrophage colony-stimulating factor (Wako, Osaka, Japan) for six days, as described previously [22]. The cells were cultured and then treated or not treated with 1 ng/mL *Escherichia coli* LPS (Sigma Aldrich) for the indicated times.

2.3. Isolation of adipose tissue fraction

To isolate the cells of the mature adipocyte fraction (MAF) and stromal vascular fraction (SVF), epididymal white adipose tissue (eWAT) was obtained from ND- or HFD-fed mice, minced, and digested in phosphate-buffered saline (PBS) containing 1 mg/mL collagenase (Sigma Aldrich) at 37 °C on a shaker until fully dissociated. The cell suspensions were filtered through a nylon strainer with a pore size of 70 μm (BD Biosciences, Bedford, MA, USA). The flow-through with cells was centrifuged at 500×*g* for 5 min at 25 °C. The floating mature adipocytes were collected as MAF. The remaining SVF cell pellet was resuspended in PBS and then pelleted (centrifugation, 500×*g*, 5 min, 25 °C).

2.4. Transient transfection

Cells were seeded in 6-well or 12-well plates at 50–60% confluence

before transfection. A miR-582-5p mimic or a control mimic and a small interfering RNA (siRNA) targeting *Skp1* or control siRNA (Supplementary Table S1) were transfected into RAW264.7 cells using Lipofectamine RNAiMAX (Invitrogen, Carlsbad, CA, USA), according to the manufacturer's instructions. The transfection was validated after 24 h by assessing the levels of the transfected miRNA or siRNA target using quantitative PCR (qPCR) or western blotting.

2.5. RNA isolation and qPCR

The total RNA content from cells or tissues was isolated and purified using ISOGEN II (Nippon Gene, Tokyo, Japan), following the manufacturer's protocol. Cells were lysed with ISOGEN II after carefully rinsing twice with PBS. The WAT samples preserved using RNAlater Stabilization Solution (Invitrogen) were gradually thawed on ice prior to the immediate homogenization in ISOGEN II using a tissue sonic homogenizer. RNA purity and concentration were measured using a microvolume spectrophotometer, NanoDrop Lite (Thermo Fisher Scientific, Waltham, MA, USA).

For mRNA quantification, 500 ng of total RNA was reverse transcribed to cDNA using the PrimeScript Master Mix reagent (Takara Bio, Shiga, Japan). LUNA Universal qPCR Master Mix (New England Biolabs, Ipswich, MA, USA) was used for the qPCR analysis on a StepOnePlus Real-Time System (Applied Biosystems, Foster, CA, USA) under the following conditions: 95 °C for 60 s, followed by 40 cycles of 95 °C for 15 s and 60 °C for 30 s.

For miRNA quantification, 500 ng of total RNA was reverse transcribed using the miScriptII RT Kit (Qiagen, Hilden, Germany). MiScript SYBR Green PCR Kit and the miScript miRNA Primer Assay (Qiagen) were used to measure miRNA expression using a mmu-miR-582-5p primer (Supplementary Table S2).

The relative amounts of mRNA and miRNA were assessed using the $2^{-\Delta\Delta Ct}$ method. Glyceraldehyde-3-phosphate dehydrogenase (*Gapdh*) and U6 small nuclear 6 (*RNU6-6P*) were used as endogenous controls for mRNA and miRNA, respectively. The primer sequences used in this study are listed in Supplementary Table S2.

2.6. Protein isolation and western blotting

For cytoplasmic protein isolation, conditioned cells were carefully washed twice with ice-cold PBS and were immediately lysed in 150 μL of CytoBuster (Novagen, Madison, WI, USA) supplemented with protease and/or phosphatase inhibitor cocktails (Nacalai Tesque), as described previously [23].

For nuclear protein extraction, NE-PER nuclear and cytoplasmic extraction reagent kit (Thermo Fisher Scientific) was used following the manufacturer's protocol. Low protein binding microcentrifuge tubes (Sarstedt, Tokyo, Japan) were used to minimize protein loss during the sample preparation, and all procedures were performed on ice. Protein concentrations were quantified using Bradford assay (Bio-Rad, Hercules, CA, USA); protein concentration-matched lysates were denatured at 70 °C for 30 min. An equal amount of protein was separated by electrophoresis using 10%, 12%, or 15% sodium dodecyl sulfate-polyacrylamide gel electrophoresis and transferred onto polyvinylidene difluoride membranes (Merck Millipore, Burlington, MA, USA). The membranes were blocked with Blocking One solution (Nacalai Tesque) and then incubated with individual primary antibodies for 1 h at room temperature or overnight at 4 °C. Next, the membranes were incubated with a secondary antibody for 1 h at room temperature. The blotted membranes were visualized using Chemi-Lumi One Super (Nacalai Tesque), and digital images were obtained using ImageQuant LAS 4000 Mini (GE Healthcare Life Sciences, Uppsala, Sweden). The band intensities were quantified using the ImageJ software (National Institutes of Health, Bethesda, MD, USA). All antibodies used are listed in Supplementary Table S3.

2.7. Enzyme-linked immunosorbent assay (ELISA)

To assess the secretion of TNF-α, IL-6, and IL-1β from macrophages following stimulation with LPS, the cell culture supernatants were collected and centrifuged at 9200×*g* at 4 °C for 5 min. Cytokine concentrations were determined using ELISA MAX Deluxe Set Mouse TNF-α, IL-6, or IL-1β kit (Biolegend, San Diego, CA, USA) according to the manufacturer's instructions.

2.8. Immunofluorescence staining

After the respective treatments, the cells were fixed with 4% paraformaldehyde phosphate buffer solution (PFA, Nacalai Tesque) for 30 min at room temperature. The fixed cells were treated with 0.5% Triton X-100 (Junsei, Tokyo, Japan) for 15 min to permeabilize the cells. The treated cells were blocked with 3% bovine serum albumin in PBS for 1 h at room temperature and stained with primary *anti*-SKP1 (1:500) or *anti*-p65 antibodies (1:1000) overnight at 4 °C. Alexa Fluor 488-conjugated goat anti-mouse or anti-rabbit IgG (Invitrogen) was used as the secondary antibody, and the membranes were incubated in the dark for 1 h at room temperature. The slides were mounted with DAPI-Fluoromount-G (SouthernBiotech, Birmingham, AL, USA). SKP1 images were captured using an all-in-one fluorescence microscope (BZ-X800, KEYENCE, Osaka, Japan), and p65 images were captured using a Nikon C2 confocal microscope (Nikon, Tokyo, Japan). The antibodies used are listed in Supplementary Table S3.

2.9. Dual-luciferase reporter gene assay

The fragment of *Skp1* 3′-UTR (WT) and its corresponding mutated sequences (MUT), designed by converting the miR-582-5p binding sequence 3′-ATGTCA to 3′-ACTCAA, were synthesized and cloned into the pmirGLO dual-luciferase miRNA Target Expression Vector (Promega, Madison, WI, USA) termed *Skp1*-3′-UTR-WT (5′-AAACTAGCGGCCGCTAGTACTGTAT) and *Skp1*-3′-UTR-MUT (5′-AAACTAGCGGCCGCTAGTAACTCAT), respectively. The plasmids were co-transfected with the miR-582-5p mimic or control miRNA into RAW264.7 cells using Lipofectamine 3000 (Invitrogen) according to the manufacturer's instructions. The luciferase activity was measured using Firefly & Renilla Luciferase Single Tube Assay Kit (Biotium, Fremont, CA, USA) and Lumat LB9508 (EG & G Berthold, Gaithersburg, MD, USA) 48 h after transfection, in line with the manufacturer's protocol. The relative luciferase activity of each sample was normalized to the activity of Renilla luciferase.

2.10. miRNA microarray analysis

Eight-week-old male C57BL/6J mice were randomized into experimental groups (n = 3 mice/group) and fed with either an ND or HFD for eight weeks. Total RNA content, including miRNAs of eWAT from the same group, was extracted using a miRNesy mini kit (Qiagen) and mixed as one sample for each group. Comprehensive miRNA expression analysis was performed using 3D-Gene Mouse miRNA (Ver.21) chips according to the protocols provided by Toray Industries (Tokyo, Japan). The annotation and oligonucleotide sequences of the probes conformed to the miRBase Release 21 database (http://microrna.sanger.ac.uk/sequences/). After repeated cycles of stringent wash steps, fluorescence signals were scanned using the 3D-Gene Scanner and analyzed using the 3D-Gene Extraction software, according to the manufacturer's protocols (Toray Industries). The raw data of each given miRNA was normalized by substitution with the mean intensity of the background signal determined by all the blank spots' signal intensities at 95% confidence intervals. Measurements of spots with signal intensities greater than two standard deviations (SDs) of the background signal intensity were considered to be valid. The relative expression level of a given miRNA was calculated by comparing the signal intensities of the valid spots

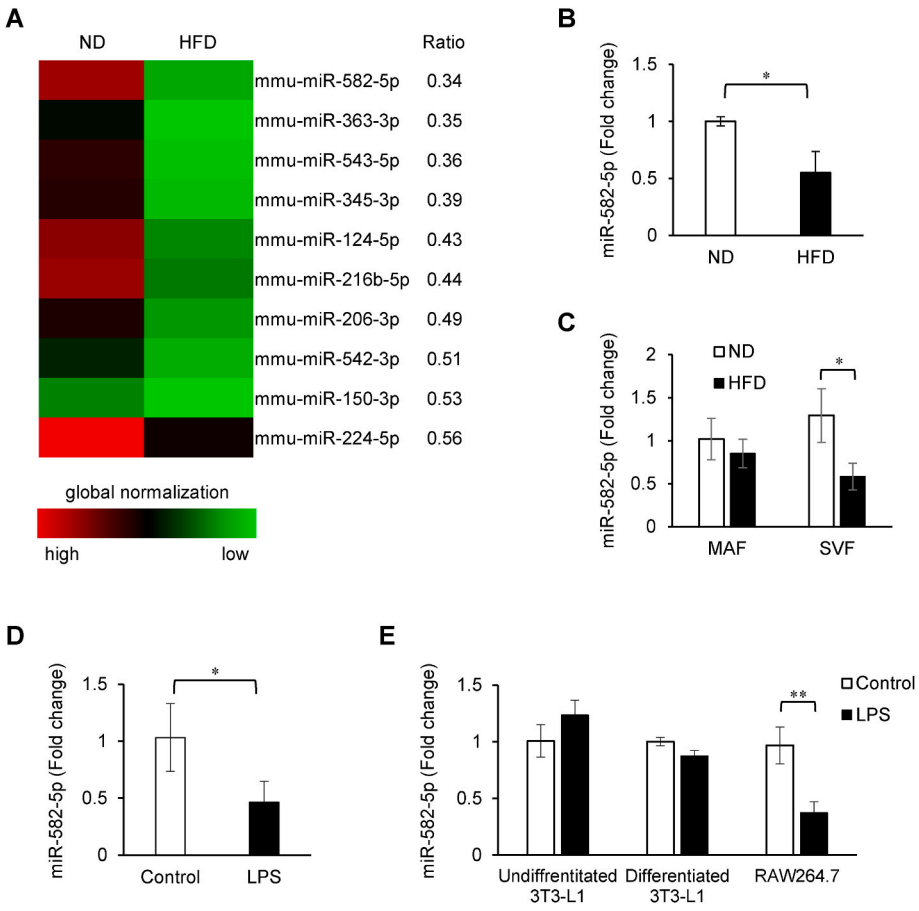

Fig. 1. High-fat diet-induced adipose tissue inflammation reduces the expression of miR-582-5p in macrophages. (A–C) Eight-week-old male C57BL/6J mice were fed with a normal diet (ND) or high-fat diet (HFD) *ad libitum* for eight weeks to induce a diet-induced obesity model. At 16 weeks of age, epididymal white adipose tissue (eWAT) was harvested for miRNA isolation, followed by microarray analysis. Heatmap of selected downregulated miRNAs in the eWAT of HFD-fed mice detected using microarray assay (A). Each point represents the value calculated using global normalization. Red and green colors represent high and low expression, respectively. The ratio is expressed as the calculated value of the HFD-fed group vs. that of the ND-fed group. Quantitative real-time PCR (qPCR) analysis of miR-582-5p abundance in eWAT (B) or the mature adipocyte fraction (MAF) and the stromal vascular fraction (SVF) of eWAT (C) from the ND- or HFD-fed mice. (D, E) miR-582-5p abundance in the bone marrow-derived macrophages from 6-week-old male C57BL/6J mice (D) or in undifferentiated and differentiated 3T3-L1 cells or RAW264.7 cells (E). Cells were incubated with or without LPS for 2 h (represented as LPS and Control in the graphs, respectively), and then miR-582-5p expression was analyzed using qPCR. *RNU6-6P* was used as the internal reference gene (B–E). The bar graph represents the mean ± SD (B–D: n = 3 for each group; E: n = 3 for each of the undifferentiated and differentiated 3T3-L1 cells or RAW264.7 cells). $^{*}p < 0.05$, $^{**}p < 0.01$ between the indicated bars of two groups (Student's *t*-test). (For interpretation of the references to color in this figure legend, the reader is referred to the Web version of this article.)

throughout the microarray experiments. The normalized data were globally normalized per array, such that the median of the signal intensity was adjusted to 25. The obtained miRNA expression profile data were deposited to the Gene Expression Omnibus database in NCBI (GSE accession: GSE216923).

2.11. Statistical analysis

All experiments were performed in triplicate. Statistical analyses were performed using JMP Pro 16 software (SAS Institute, Cary, NC, USA). Paired analyses were performed using Student's *t*-test, while multiple group analyses were performed using Tukey-Kramer's HSD test. Values are presented as mean ± SD. A p-value<0.05 was considered statistically significant.

3. Results

3.1. High-fat diet-induced adipose tissue inflammation reduces the expression of miR-582-5p in macrophages

To identify novel miRNAs that regulate obesity-induced inflammation in adipose tissues, we performed miRNA microarray analysis using the RNA of eWAT obtained from the HFD- or ND-fed mice. The phenotypes of the mice used are listed in Supplementary Fig. S1. We identified miRNAs that were downregulated in the eWAT of HFD-fed mice compared with that in their ND-fed littermates (Fig. 1A). Among these miRNAs, we observed that miR-582-5p was the most downregulated (0.34-fold) in the eWAT of the HFD-fed mice compared to that in their ND-fed littermates. miR-582-5p is involved in inflammatory processes [24,25]. However, the detailed mechanism remains unclear. Therefore, we examined the role of miR-582-5p in regulating inflammation.

miR-582-5p expression was significantly lower in the eWAT from the HFD-fed mice than that in that from the ND-fed mice (Fig. 1B). To determine the cellular source of miR-582-5p decrease in obesity, we fractionated eWAT into MAF and SVF. The expression of miR-582-5p was markedly downregulated in the SVF of eWAT obtained from HFD-fed mice, while there was no significant expression change in miR-582-5p in the MAF (Fig. 1C). We evaluated the miR-582-5p expression in bone marrow-derived macrophages; miR-582-5p expression was downregulated in LPS-treated macrophages (Fig. 1D).

We further examined miR-582-5p expression in 3T3-L1 preadipocytes, differentiated 3T3-L1 adipocytes, and RAW264.7 cells (murine macrophage cells). Following stimulation with LPS, neither 3T3-L1 preadipocytes nor differentiated 3T3-L1 adipocytes displayed a significant change in miR-582-5p expression (Fig. 1E). Meanwhile, the expression of miR-582-5p in RAW264.7 was significantly attenuated (Fig. 1E). Therefore, miR-582-5p could play a potential role in the regulation of LPS-induced inflammatory process in macrophages.

3.2. miR-582-5p attenuates LPS-induced inflammatory cytokine production in RAW264.7 cells

Next, we examined the effect of miR-582-5p on the production of cytokines such as TNF-α, IL-1β, and IL-6 in RAW264.7 cells. The miR-582-5p mimic significantly inhibited the LPS-induced transcription (Fig. 2A) and protein (Fig. 2B) expression of TNF-α, IL-1β, and IL-6 in RAW264.7 cells. The concentrations of TNF-α, IL-1β, and IL-6 in the culture medium were also reduced (Fig. 2C). Therefore, miR-582-5p could ameliorate the production of inflammatory cytokines in macrophages.

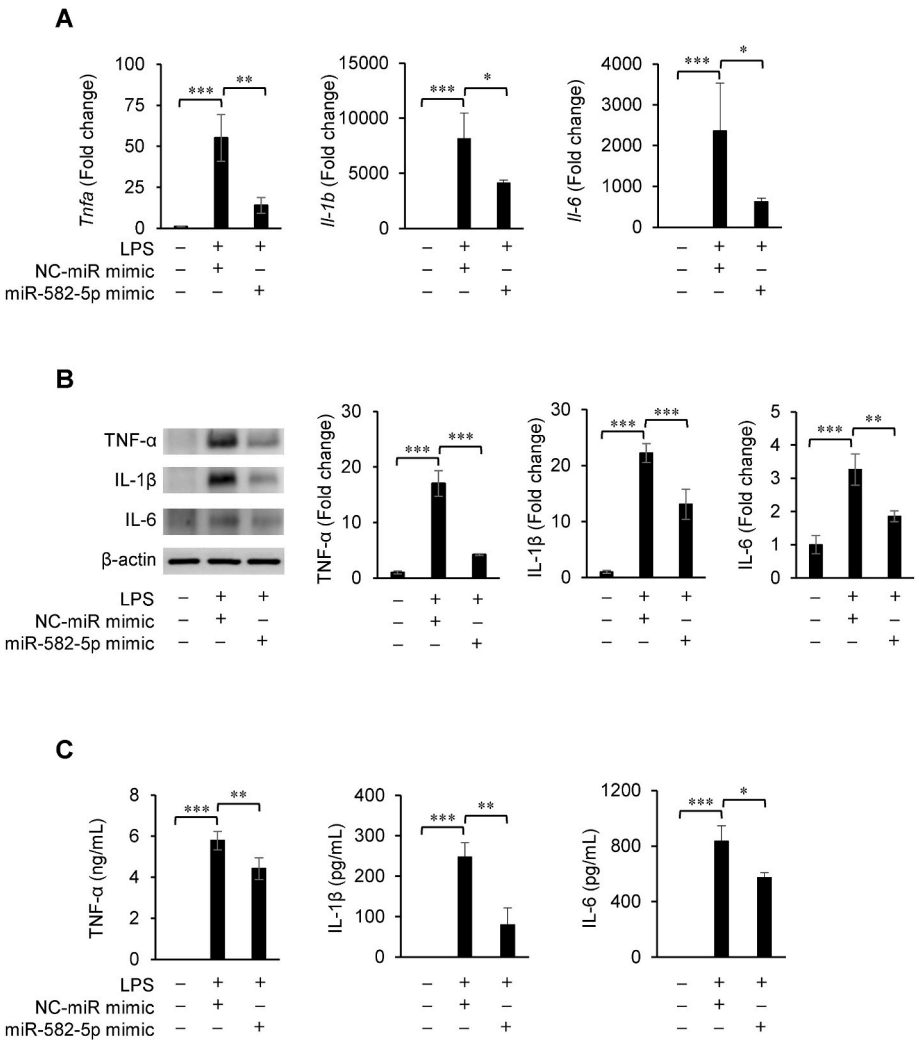

Fig. 2. miR-582-5p attenuates LPS-induced inflammatory cytokine production in RAW264.7 cells. (A–C) RAW264.7 cells were transfected with the miR-582-5p mimic (20 nM) or the negative control microRNA mimic (NC-miR mimic, 20 nM) for 24 h and incubated with or without LPS for 2 h (A), 4 h (B), and 48 h (C). Then, mRNA (A), protein lysates (B), and supernatants (C) were harvested for subsequent analyses. mRNA (A) and protein (B, C) expression of TNF-α, IL-1β, and IL-6 were measured using qPCR (A), western blotting (B), and ELISA (C). We repeated this experiment thrice. A set of representative blots from three independent experiments are shown (B), and two other images are presented in Supplementary Fig. S2. *Gapdh* was used as the internal reference gene (A). β-actin was used as the loading control (B). Bar graphs represent the mean ± SD (A–C, n = 3 for each group). $^{*}p < 0.05$, $^{**}p < 0.01$, $^{***}p < 0.001$ represent significant differences between the indicated bars (Tukey-Kramer's HSD-test).

3.3. *Skp1* is a direct target of miR-582-5p

We used TargetScan (release 7.2) to predict the potential candidate targets of miR-582-5p. We screened several genes related to the NF-κB signaling pathway, a major signaling pathway involved in inflammatory responses. Their expression in RAW264.7 cells transfected with a miR-582-5p mimic or a negative control microRNA (NC-miR) mimic was measured. Exogenous miR-582-5p significantly suppressed the mRNA expression of *Skp1* but not that of other potential target genes compared to their expression in the control (Supplementary Fig. S3A). In contrast, the miR-582-5p inhibitor significantly increased *Skp1* expression (Supplementary Fig. S3B).

A putative binding site for miR-582-5p within the 3′-UTR sequence of *Skp1* was identified using TargetScan (Fig. 3A). Dual-luciferase reporter assay was used to confirm the physical binding of miR-582-5p to the *Skp1* mRNA. Inserts harboring the predicted *Skp1* wildtype sequence (*Skp1*-WT) and its mutated sequence (*Skp1*-Mut) were cloned into a luciferase reporter vector. Co-transfection of *Skp1*-WT with the miR-582-5p mimic in RAW264.7 cells showed a significant decrease in the relative luciferase activity compared with that in the negative control microRNA mimic (NC-miR mimic) group. This was not observed in the experiments using *Skp1*-Mut (Fig. 3B). This confirmed the preferential binding of miR-582-5p to the 3′-UTR site on *Skp1*. In most cases, there was an inverse correlation between miRNAs and their target mRNAs; therefore, the mRNA expression of *Skp1* in LPS-stimulated RAW264.7 cells was measured. *Skp1* mRNA expression was markedly upregulated in LPS-stimulated RAW264.7 cells (Supplementary Fig. S3C).

We evaluated the SKP1 expression in RAW264.7 cells transfected with the miR-582-5p mimic using immunofluorescence staining and western blotting. The signal intensity of SKP1 was lower in RAW264.7 cells transfected with the miR-582-5p mimic than in cells transfected with the NC-miR mimic (Fig. 3C, the DAPI [blue] images are shown in Supplementary Fig. S3D). SKP1 expression was significantly reduced in RAW264.7 cells transfected with miR-582-5p mimic (Fig. 3D).

To determine whether miR-582-5p affects the other components of $SCF^{\beta TrCP}$, the SCF complex that plays a crucial role in NF-κB signaling (i.e., polyubiquitination of phospho-IκBα), we examined the effects of the miR-582-5p mimic on the expression of these components, such as beta transducin repeat-containing protein (βTrCP), CUL1, and ring-box 1 (RBX1). However, miR-582-5p had no effect on their expression (Supplementary Fig. S4). We could not identify any potential binding sites for miR-582-5p in these genes using TargetScan analysis. Therefore, among the components of $SCF^{\beta TrCP}$ ubiquitin E3 ligase complex, only SKP1 was regulated by miR-582-5p.

3.4. *Silencing of Skp1 and expression of miR-582-5p suppresses LPS-induced NF-κB signaling pathway*

SKP1 is an integral component of the SCF ubiquitin E3 ligase; it functions as the adaptor protein responsible for connecting CUL1 and the various F-box proteins for the formation of the SCF complex. It functions in the ubiquitin-mediated degradation of IκBα in the canonical

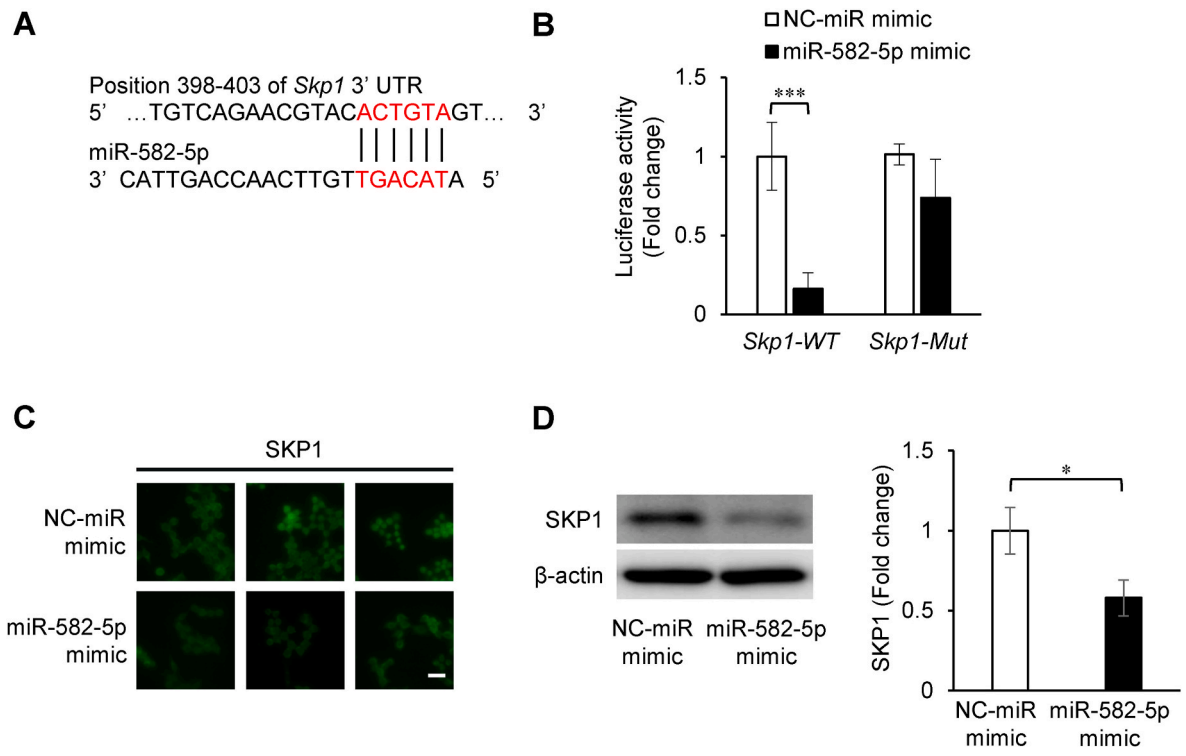

Fig. 3. *Skp1* is a direct target of miR-582-5p. (A) Sequence alignment of the potential miR-582-5p binding sites (in red letters) on S-phase kinase-associated protein 1 (*Skp1*, NM_011543.4) 3′-UTR was predicted using TargetScan (release 7.2) analysis. (B) The luciferase reporter vectors containing the wildtype miR-582-5p binding sites of *Skp1* (*Skp1*-WT) or a mutated *Skp1* sequence (*Skp1*-Mut) were co-transfected with the negative control microRNA mimic (NC-miR mimic, 20 nM) or miR-582-5p mimic (20 nM) into RAW264.7 cells. After 48 h, firefly luciferase activity in each sample was measured and normalized to the control (Renilla) luciferase activity. (C, D) RAW264.7 cells were transfected with the NC-miR mimic (20 nM) or miR-582-5p mimic (20 nM) for 24 h. Representative images of immunofluorescence staining for endogenous SKP1 (green) from three independent assays (C). DAPI (blue) images are presented in Supplementary Fig. S3D. Scale bar = 20 μm. SKP1 expression was analyzed using western blotting (D). A set of representative blots from three independent experiments are shown. Two other data sets are presented in Supplementary Fig. S3E β-actin was used as the loading control. Bar graphs represent the mean ± SD (B, D: n = 3 for each group). *$p < 0.05$, ***$p < 0.001$ between the indicated bars of two groups (Student's *t*-test). (For interpretation of the references to color in this figure legend, the reader is referred to the Web version of this article.)

NF-κB signaling pathway (Fig. 4A). To evaluate the role of SKP1 in NF-κB signaling, RAW264.7 cells were transfected with siRNA specific for SKP1 (si-*Skp1*) and stimulated with LPS for 90 min *Skp1* silencing inhibited LPS-induced degradation of IκBα and phosphorylation of NF-κB p65 (Fig. 4B), along with the nuclear translocation of NF-κB p65 (Fig. 4C).

To investigate the biological functions of miR-582-5p in NF-κB signaling, RAW264.7 cells were transfected with an NC-miR mimic or a miR-582-5p mimic and stimulated with LPS for activating the NF-κB pathway. Western blotting revealed that the expression of the miR-582-5p mimic reduced SKP1 expression (see Fig. 4D, the far-left upper panel). This attenuated LPS-induced IκBα degradation and NF-κB p65 phosphorylation in RAW264.7 cells compared to that in cells expressing the NC-miR mimic (Fig. 4D). Furthermore, LPS-inducible NF-κB p65 nuclear translocation was significantly suppressed in the miR-582-5p mimic transfection group compared with that in the NC-miR mimic transfection group (Fig. 4E). Immunocytochemistry analysis indicated that p65 signals were localized to the nucleus in response to LPS stimulation; this was substantially inhibited in the miR-582-5p mimic-transfected cells (Fig. 4F and Supplementary Fig. S7). Therefore, miR-582-5p attenuated the inflammatory response of LPS-stimulated macrophages *via* NF-κB signaling inhibition by targeting *Skp1*.

4. Discussion

In this study, miR-582-5p decreased under the inflammatory state, inhibited degradation of IκBα in the NF-κB pathway, and suppressed pro-inflammatory cytokine expression in macrophages by targeting *Skp1*. This could offer a novel gene therapy approach for regulating inflammation. The NF-κB pathway plays an important role in the pathogenesis of various inflammatory diseases by regulating cytokine-inducible gene expression [6]. It is important to clarify the molecular mechanisms underlying NF-κB signaling for preventing and treating inflammation. In the innate immune system, the activation of the NF-κB pathway is involved in the macrophage-associated inflammatory response induced by TLRs. LPS, an outer-membrane component of gram-negative bacteria, can migrate from the gut into circulation during pathological conditions and prime the innate immune response *via* TLR4 [26]. A high dose of LPS (0.1–1 μg/mL) leads to a hyporesponsive state of macrophages, while a subclinical low-dose LPS (0.1–1 ng/mL) induces a low-grade inflammatory state characterized by prolonged expression of inflammatory mediators such as TNF-α. Low-dose LPS is associated with chronic inflammatory pathologies such as obesity [27]. The main cell components of obese adipose tissue were preadipocytes and adipose tissue macrophages in SVF, and mature adipocytes in MAF [28]. miR-582-5p was significantly downregulated in the SVF of the obese adipose tissue and in murine macrophages induced by a low concentration of LPS (1 ng/mL).

miRNAs are potent regulators of diverse biological processes including inflammation, cell cycle, and cancer [29]. miRNAs are intensively investigated for their role in the NF-κB pathway [30,31]. miR-24 inhibited NF-κB signaling and TNF-α production by targeting high mobility group protein B1 [32]. miR-132 negatively regulates NF-κB translocation by targeting acetylcholinesterase [33]. This study indicates that there is a direct correlation between miR-582-5p and *Skp1*, which is implicated in the degradation of IκBα during the activation of the NF-κB pathway.

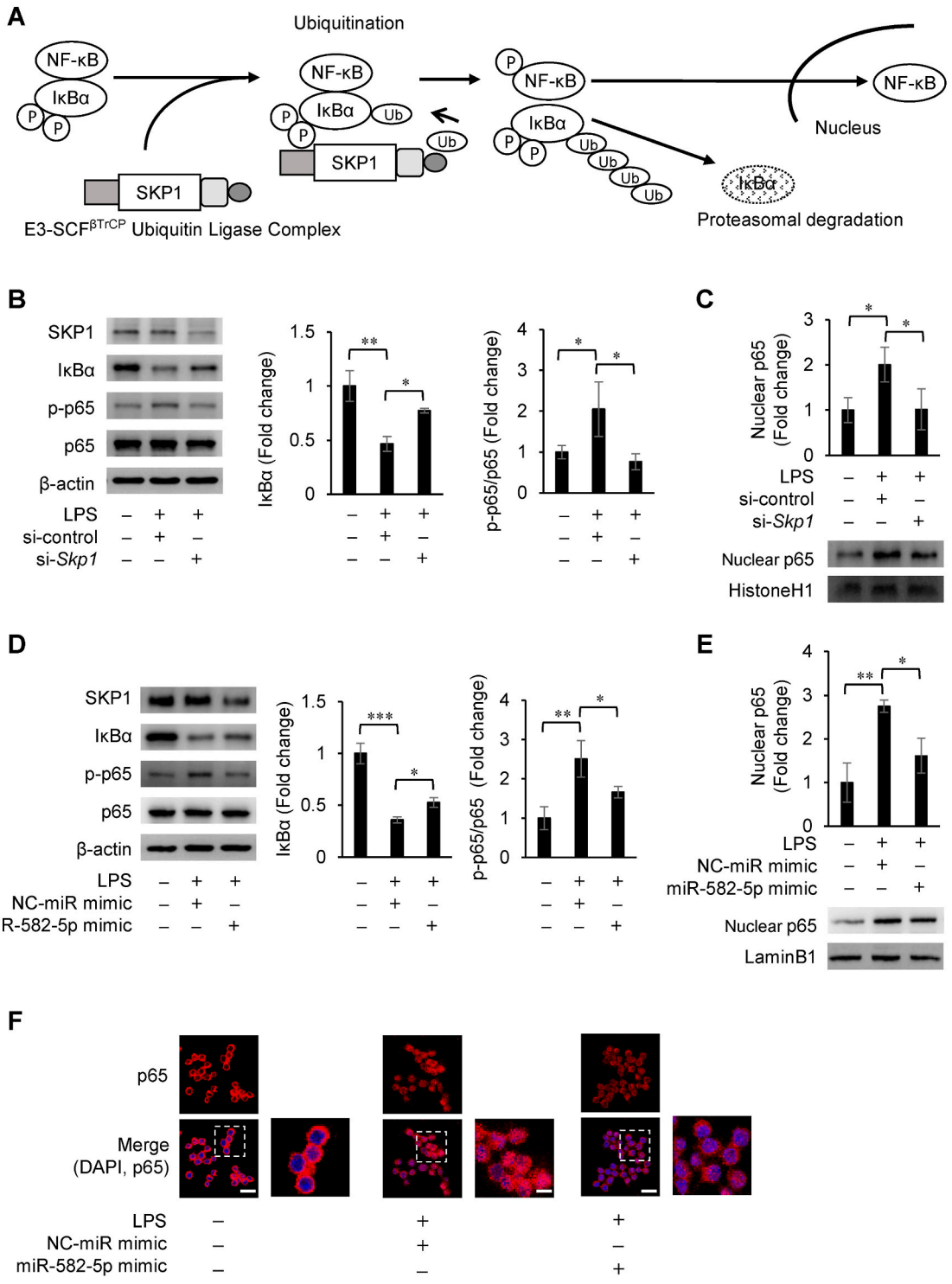

Fig. 4. Silencing of *Skp1* and expression of miR-582-5p suppresses LPS-induced NF-κB signaling. (A) Schematic illustration of SKP1-regulated canonical NF-κB signaling. (B, C) RAW264.7 cells were transfected with siRNA of *Skp1* (si-*Skp1*, 20 nM) or si-control (20 nM) for 24 h and then incubated with or without LPS for 90 min. Cell lysates (B) or nuclear fraction (C) were analyzed through western blotting using specific antibodies. A set of representative blots from three independent experiments are shown (B, C). Two other data sets are presented in Supplementary Figs. S5A and B. (D–F) RAW264.7 cells were transfected with the miR-582-5p mimic (20 nM) or negative control microRNA mimic (NC-miR mimic, 20 nM) for 24 h and then incubated with or without LPS for 90 min. Cell lysates (D) or nuclear fraction (E) were analyzed through western blotting (D, E) and immunofluorescence staining (F) using specific antibodies. A set of representative blots from three independent experiments are shown (D, E). Two other data sets are presented in Supplementary Figs. S6A and B β-actin (B, D), histone H1 (C), and lamin B1 (E) were used as the loading control. Representative images of p65 immunofluorescence staining (red) are shown in (F), and the other two sets are shown in Supplementary Fig. S7. The nuclei were counterstained with DAPI (blue). Dotted square areas in the merged images are enlarged and shown on the right side of each merged image. Scale bar = 20 μm. Bar graphs represent the mean ± SD (B–E, n = 3 for each group). *$p < 0.05$, **$p < 0.01$, ***$p < 0.001$ between the indicated bars (Tukey-Kramer's HSD-test). (For interpretation of the references to color in this figure legend, the reader is referred to the Web version of this article.)

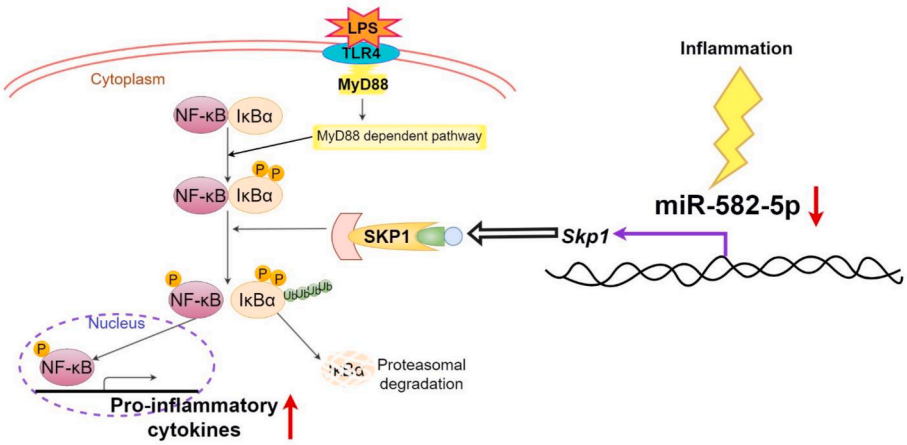

Fig. 5. A schematic representation of the molecular mechanism involved in miR-582-5p-related inflammation in macrophages. miR-582-5p is downregulated in macrophages in response to inflammation; this promotes *Skp1* gene expression followed by protein expression. SKP1 promotes the progression of the NF-κB signaling pathway by inducing the degradation of IκBα; this induces the production of pro-inflammatory cytokines such as TNF-α and IL-1β. IκBα: nuclear factor of kappa light polypeptide gene enhancer in B-cells inhibitor, alpha; LPS: lipopolysaccharide; MyD88: myeloid differentiation primary response gene 88; SKP1: S-phase kinase-associated protein 1; TLR 4: Toll-like receptor 4.

miR-582-5p is an effective tumor suppressor in non-small cell lung cancer by targeting yes-associated protein/WW domain-containing transcription regulator 1 signaling [34]. miR-582-5p, targeting collagen type V alpha 1, inhibits the progression of clear cell renal carcinoma [35]. miR-582-5p suppresses prostate cancer metastasis by regulating transforming growth factor β signaling [36]. miR-582-5p alleviates the opioid receptor-dependent effect of morphine by targeting cAMP response element-binding protein 1 [37]. Furthermore, miR-582-5p suppresses non-small cell lung cancer growth and invasion by downregulating neurogenic locus notch homolog protein 1 [38]. However, the functional and molecular mechanisms underlying the role of miR-582-5p in LPS-inducible TLR4-NF-κB signaling remained elusive. In this study, we characterized a miR-582-5p-based regulatory network that regulates NF-κB signaling activity and the inflammatory response in murine macrophages. miR-582-5p is significantly downregulated in the inflamed murine macrophages and in RAW264.7 cells under the LPS challenge, indicating that miR-582-5p participates in the regulation of inflammation and LPS-induced TLR4-NF-κB signaling.

The innate immune cells such as macrophages employ PRRs for the detection of invading microbes. TLR4, one of the PRRs, recognizes LPS and is closely involved in the activation of the NF-κB pathway [39]. miR-582-5p could attenuate the inflammatory response induced by LPS by negatively modulating SKP1 *via* directly binding to the 3′-UTR region of *Skp1* in RAW264.7 cells. SKP1 is a fixed and indispensable component and irreplaceable in the assembly of the SCF complex. In the SCF complex, SKP1 functions as an adaptor to connect CUL1 and various kinds of F-box proteins and can potentiate the substrate-binding ability of F-box proteins [40]. Targeting SKP1 is considered a potential therapeutic strategy [10]. 6-O-angeloylplenolin, a compound isolated from the herb *Centipeda minima*, competitively dissociates βTrCP (an F-box protein) from SKP1 without affecting *Skp1* expression, leading to the upregulation of its substrates such as IκBα [40]. Aberrant SKP1 is associated with several human disorders, including sporadic Parkinson's disease [41], and cancer [42]. However, when the NF-κB signaling pathway is activated, $SCF^{\beta TrCP}$, the SCF complex with the F-box protein βTrCP, induces the polyubiquitination of phosphorylated IκBα; this leads to its degradation by the proteasome. The NF-κB p65/p50 heterodimer is liberated, and it subsequently translocates into the nucleus to induce the transcription of various genes, including those encoding inflammatory cytokines such as *Tnfa*, *Il-6*, and *Il-1β* [43,44]. Hyperactivation of the NF-κB signaling pathway *via* MyD88 is implicated in the cytokine storm associated with coronavirus disease 2019 (COVID-19) [45–47]. We confirmed that miR-582-5p by targeting *Skp1* could ameliorate the activation of NF-κB and the production of inflammatory cytokines (TNF-α, IL-1β, and IL-6) by inhibiting the degradation of IκBα. Therefore, overexpression of miR-582-5p could be a potential strategy for improving NF-κB signaling.

5. Conclusion

miR-582-5p, a miRNA that decreases during inflammation, could inhibit LPS-induced inflammatory response *via* suppressing NF-κB signaling by targeting *Skp1* (Fig. 5). Therefore, regulation of miR-582-5p could be a therapeutic strategy for inflammation-related pathologies.

Author contributions

Conceptualization: Rongzhi Li, Tomomi Sano;
Data curation: Rongzhi Li, Tomomi Sano;
Formal analysis: Rongzhi Li, Tomomi Sano;
Funding acquisition: Tomomi Sano;
Investigation: Rongzhi Li, Tomomi Sano;
Methodology: Rongzhi Li, Tomomi Sano, Akiko Mizokami, Takashi Kanematsu, Fusanori Nishimura;
Project administration: Tomomi Sano, Takashi Kanematsu, Fusanori Nishimura;
Resources: Tomomi Sano, Akiko Mizokami, Yusuke Nakatsu, Yusuke Sotomaru, Tomoichiro Asano;
Software: Rongzhi Li, Tomomi Sano;
Supervision: Tomomi Sano, Fusanori Nishimura;
Validation: Takao Fukuda, Takanori Shinjo, Misaki Iwashita, Akiko Yamashita, Terukazu Sanui;
Visualization: Tomomi Sano;
Roles/Writing - original draft: Rongzhi Li, Tomomi Sano;
Writing - review & editing: Takashi Kanematsu, Fusanori Nishimura.

Funding

This work was supported by a Grant-in-Aid from the Japan Society for the Promotion of Science [grant number 20K18512].

Declaration of competing interest

None.

Data availability

Data will be made available on request.

Acknowledgments

We appreciate the technical assistance from The Research Support Center, Research Center for Human Disease Modeling, Kyushu University Graduate School of Medical Sciences.

Appendix A. Supplementary data

Supplementary data to this article can be found online at https://doi.org/10.1016/j.abb.2022.109501.

References

[1] T. Lawrence, The nuclear factor NF-kappaB pathway in inflammation, Cold Spring Harbor Perspect. Biol. 1 (2009), 001651.
[2] H. Wu, C.M. Ballantyne, Metabolic inflammation and insulin resistance in obesity, Circ. Res. 126 (2020) 1549–1564.
[3] C. Nathan, A. Ding, Nonresolving inflammation Cell. 140 (2010) 871–882.
[4] E.A. Ross, A. Devitt, J.R. Johnson, Macrophages: the good, the bad, and the gluttony, Front. Immunol. 12 (2021), 708186.
[5] S. Watanabe, M. Alexander, A.V. Misharin, G. Budinger, The role of macrophages in the resolution of inflammation, J. Clin. Invest. 129 (2019) 2619–2628.
[6] T. Liu, L. Zhang, D. Joo, S.C. Sun, NF-κB signaling in inflammation, Signal Transduct. Targeted Ther. 2 (2017), 17023.
[7] A. Kauppinen, T. Suuronen, J. Ojala, K. Kaarniranta, A. Salminen, Antagonistic crosstalk between NF-κB and SIRT1 in the regulation of inflammation and metabolic disorders, Cell. Signal. 25 (2013) 1939–1948.
[8] L. Catrysse, G. van Loo, Inflammation and the metabolic syndrome: the tissue-specific functions of NF-κB, Trends Cell Biol. 27 (2017) 417–429.
[9] L. Barnabei, E. Laplantine, W. Mbongo, F. Rieux-Laucat, R. Weil, NF-κB: at the borders of autoimmunity and inflammation, Front. Immunol. 12 (2021), 716469.
[10] L.L. Thompson, K.A. Rutherford, C.C. Lepage, K.J. McManus, Aberrant SKP1 expression: diverse mechanisms impacting genome and chromosome stability, Front. Cell Dev. Biol. 10 (2022), 859582.
[11] B. Huang, X.D. Yang, A. Lamb, L.F. Chen, Posttranslational modifications of NF-kappaB: another layer of regulation for NF-kappaB signaling pathway, Cell. Signal. 22 (2010) 1282–1290.
[12] D.P. Bartel, Metazoan microRNAs, Cell 173 (2018) 20–51.
[13] A. Tahamtan, M. Teymoori-Rad, B. Nakstad, V. Salimi, Anti-inflammatory microRNAs and their potential for inflammatory diseases treatment, Front. Immunol. 9 (2018) 1377.
[14] S.M. Hammond, An overview of microRNAs, Adv. Drug Deliv. Rev. 87 (2015) 3–14.
[15] J. Wu, J. Ding, J. Yang, X. Guo, Y. Zheng, MicroRNA roles in the nuclear factor kappa B signaling pathway in cancer, Front. Immunol. 9 (2018) 546.
[16] Y. Zou, Y. Cai, D. Lu, Y. Zhou, Q. Yao, S. Zhang, MicroRNA-146a-5p attenuates liver fibrosis by suppressing profibrogenic effects of TGFβ1 and lipopolysaccharide, Cell. Signal. 39 (2017) 1–8.
[17] K.D. Taganov, M.P. Boldin, K.J. Chang, D. Baltimore, NF-kappaB-dependent induction of microRNA miR-146, an inhibitor targeted to signaling proteins of innate immune responses, Proc. Natl. Acad. Sci. U. S. A. 103 (2006) 12481–12486.
[18] T. Sanada, T. Sano, Y. Sotomaru, R. Alshargabi, Y. Yamawaki, A. Yamashita, et al., Anti-inflammatory effects of miRNA-146a induced in adipose and periodontal tissues, Biochem. Biophys. Rep. 22 (2020), 100757.
[19] M. Ju, B. Liu, H. He, Z. Gu, Y. Liu, Y. Su, et al., MicroRNA-27a alleviates LPS-induced acute lung injury in mice via inhibiting inflammation and apoptosis through modulating TLR4/MyD88/NF-κB pathway, Cell Cycle 17 (2018) 2001–2018.
[20] T. Sano, M. Iwashita, S. Nagayasu, A. Yamashita, T. Shinjo, A. Hashikata, et al., Protection from diet-induced obesity and insulin resistance in mice lacking CCL19-CCR7 signaling, Obesity 23 (2015) 1460–1471.
[21] T. Sano, S. Nagayasu, S. Suzuki, M. Iwashita, A. Yamashita, T. Shinjo, et al., Epicatechin downregulates adipose tissue CCL19 expression and thereby ameliorates diet-induced obesity and insulin resistance, Nutr. Metabol. Cardiovasc. Dis. 27 (2017) 249–259.
[22] Y.C. Chen, Y.S. Lai, Y.D. Hsuuw, K.T. Chang, Withholding of M-CSF supplement reprograms macrophages to M2-like via endogenous CSF-1 activation, Int. J. Mol. Sci. 22 (2021) 3532.
[23] T. Sano, T. Sanada, Y. Sotomaru, T. Shinjo, M. Iwashita, A. Yamashita, et al., Ccr7 null mice are protected against diet-induced obesity via Ucp1 upregulation and enhanced energy expenditure, Nutr. Metab. 16 (2019) 43.
[24] J. Mei, Y. Zhang, S. Lu, J. Wang, Long non-coding RNA NNT-AS1 regulates proliferation, apoptosis, inflammation and airway remodeling of chronic obstructive pulmonary disease via targeting miR-582-5p/FBXO11 axis, Biomed. Pharmacother. 129 (2020), 110326.
[25] Y. Zhang, X. Zhang, Z. Zhao, Y. Zheng, Z. Xiao, F. Li, Integrated bioinformatics analysis and validation revealed potential immune-regulatory miR-892b, miR-199b-5p and miR-582-5p as diagnostic biomarkers in active tuberculosis, Microb. Pathog. 134 (2019), 103563.
[26] F.Y. Liew, D. Xu, E.K. Brint, L.A.J. O'Neill, Negative regulation of toll-like receptor-mediated immune responses, Nat. Rev. Immunol. 5 (2005) 446–458.
[27] A. Rahtes, L. Li, Polarization of low-grade inflammatory monocytes through TRAM-mediated up-regulation of Keap1 by super-low dose endotoxin, Front. Immunol. 11 (2020) 1478.
[28] A. Chait, L.J. den Hartigh, Adipose tissue distribution, inflammation and its metabolic consequences, including diabetes and cardiovascular disease, Front. Cardiovasc. Med. 7 (2020) 22.
[29] D. Sayed, M. Abdellatif, MicroRNAs in development and disease, Physiol. Rev. 91 (2011) 827–887.
[30] X. Ma, L.E. Becker Buscaglia, J.R. Barker, Y. Li, MicroRNAs in NF-kappaB signaling, J. Mol. Cell Biol. 3 (2011) 159–166.
[31] M.P. Boldin, D. Baltimore, MicroRNAs, new effectors and regulators of NF-κB, Immunol. Rev. 246 (2012) 205–220.
[32] J. Yang, L. Chen, J. Ding, Z. Fan, S. Li, H. Wu, et al., MicroRNA-24 inhibits high glucose-induced vascular smooth muscle cell proliferation and migration by targeting HMGB1, Gene 586 (2016) 268–273.
[33] F. Liu, Y. Li, R. Jiang, C. Nie, Z. Zeng, N. Zhao, et al., miR-132 inhibits lipopolysaccharide-induced inflammation in alveolar macrophages by the cholinergic anti-inflammatory pathway, Exp. Lung Res. 41 (2015) 261–269.
[34] B. Zhu, M. V, M. Finch-Edmondson, Y. Lee, Y. Wan, M. Sudol, R. DasGupta, miR-582-5p is a tumor suppressor microRNA targeting the Hippo-YAP/TAZ signaling pathway in non-small cell lung cancer, Cancers 13 (2021) 756.
[35] J. Xue, S. Zhu, F. Qi, K. Zhu, P. Cao, J. Yang, et al., RUNX1/miR-582-5p pathway regulates the tumor progression in clear cell renal cell carcinoma by targeting COL5A1, Front. Oncol. 11 (2021), 610992.
[36] S. Huang, C. Zou, Y. Tang, Q. Wa, X. Peng, X. Chen, et al., miR-582-3p and miR-582-5p suppress prostate cancer metastasis to bone by repressing TGF-β signaling, Mol. Ther. Nucleic Acids 16 (2019) 91–104.
[37] X. Long, Y. Li, S. Qiu, J. Liu, L. He, Y. Peng, miR-582-5p/miR-590-5p targeted CREB1/CREB5-NF-κB signaling and caused opioid-induced immunosuppression in human monocytes, Transl. Psychiatry 6 (2016) 757.
[38] J. Liu, S. Liu, X. Deng, J. Rao, K. Huang, G. Xu, et al., MicroRNA-582-5p suppresses non-small cell lung cancer cells growth and invasion via downregulating NOTCH1, PLoS One 14 (2019), 0217652.
[39] T. Kawai, S. Akira, The role of pattern-recognition receptors in innate immunity: update on Toll-like receptors, Nat. Immunol. 11 (2010) 373–384.
[40] M. Hussain, Y. Lu, Y.Q. Liu, K. Su, J. Zhang, J. Liu, et al., Skp1: implications in cancer and SCF-oriented anti-cancer drug discovery, Pharmacol. Res. 111 (2016) 34–42.
[41] S.A. Mandel, T. Fishman-Jacob, M.B. Youdim, Targeting SKP1, an ubiquitin E3 ligase component found decreased in sporadic Parkinson's disease, Neurodegener. Dis. 10 (2012) 220–223.
[42] J.S. Silverman, J.R. Skaar, M. Pagano, SCF ubiquitin ligases in the maintenance of genome stability, Trends Biochem. Sci. 37 (2012) 66–73.
[43] Z.J. Chen, Ubiquitin signalling in the NF-kappaB pathway, Nat. Cell Biol. 7 (2005) 758–765.
[44] B. Hoesel, J.A. Schmid, The complexity of NF-κB signaling in inflammation and cancer, Mol. Cancer 12 (2013) 86.
[45] R. Kircheis, E. Haasbach, D. Lueftenegger, W.T. Heyken, M. Ocker, O. Planz, NF-κB pathway as a potential target for treatment of critical stage COVID-19 patients, Front. Immunol. 11 (2020), 598444.
[46] A. Hariharan, A.R. Hakeem, S. Radhakrishnan, M.S. Reddy, M. Rela, The role and therapeutic potential of NF-kappa-B pathway in severe COVID-19 patients, Inflammopharmacology 29 (2021) 91–100.
[47] A. Attiq, L.J. Yao, S. Afzal, M.A. Khan, The triumvirate of NF-κB, inflammation and cytokine storm in COVID-19, Int. Immunopharm. 101 (2021), 108255.

Supplementary Table S1. List of miRNA mimics and siRNAs used for transfection

miRNA	Catalog number	Source
mmu-miR-582-5p miRCURY LNA miRNA mimic	YM00471571	Qiagen, Hilden, Germany
control miRCURY LNA miRNA mimic	YM00479902	Qiagen, Hilden, Germany
siRNA		
*Skp*1-siRNA	MSS277837	Invitrogen, Carlsbad, CA, USA
control siRNA	S10C-0600	Cosmo Bio, Tokyo, Japan

Supplementary Table S2. Sequence of primers used in this study

Gene name		Sequence
Gapdh	forward	5′-AATGTGTCCGTCGTGGATCTGA-3′
	reverse	5′-GATGCCTGCTTCACCACCTTCT-3′
Myd88	forward	5′-AGGACAAACGCCGGAACTTTT-3′
	reverse	5′-GCCGATAGTCTGTCTGTTCTAGT-3′
Irak4	forward	5′-CCTGGATGTCCTGGAACTTG-3′
	reverse	5′-CAACACGCAGTAGGCAGAGA-3′
Traf6	forward	5′-ACTGGGGACAATTCACTAGAGC-3′
	reverse	5′-AAAGCGAGAGATTCTTTCCCTG-3′
Tak1	forward	5′-AGGTTGTCGGAAGAGGAGCT-3′
	reverse	5′-CTCCACAATGAAAGCCTTCC-3′
Tab1	forward	5′-ACCCTGCTGGTGAGGAACT-3′
	reverse	5′-AGGGACAGAGTCACACTAGTCT-3′
Tab2	forward	5′-GGATAGAATAAGCGAAGCCCGGAA-3′
	reverse	5′-CTCTTTGAAGCCGTTCCATCCT-3′
Skp1	forward	5′-ATGCCTACGATAAAGTTGCAGA-3′
	reverse	5′-TCCATTCCCAAATCTTCCAGC-3′
Tnfa	forward	5′-CATGGATCTCAAAGACAACC-3′
	reverse	5′-GGTATATGGGCTCATACCAG-3′
Il-1b	forward	5′-GAAGAAGAGCCCATCCTCTG-3′
	reverse	5′-TCATCTCGGAGCCTGTAGTG-3′
Il-6	forward	5′-TGCCTTCTTGGGACTGATG-3′
	reverse	5′-ACTCTGGCTTTGTCTTTCTTGT-3′
RNU6-6P		5′-CGCAAGGATGACACGCAAATTCGT-3′
mmu-miR-582-5p		5′-GGTATATGGGCTCATACCAG-3′

Gapdh: glyceraldehyde-3-phosphate dehydrogenase; *Myd88*: myeloid differentiation primary response gene 88; *Irak4*: interleukin-1 receptor-associated kinase 4; *Traf6*: TNF receptor-associated factor 6; *Tak1*: mitogen-activated protein kinase kinase kinase 7; *Tab1*: TGF-beta activated kinase 1/MAP3K7 binding protein 1; *Tab2*: TGF-beta activated kinase 1/MAP3K7 binding protein 2; *Skp1*: S-phase kinase-associated protein 1; *Tnfa*: tumor necrosis factor-alpha; *Il-1b*: interleukin-1b; *Il-6*: interleukin-6; *RNU6-6P*: U6 small nuclear 6

Supplementary Table S3. List of antibodies used in western blotting and immunofluorescence staining

Antibody (Catalog number)	Source
TNF-α (AB-401-NA)	R&D Systems, Minneapolis, MN, USA
IL-1β /IL-1F2 (AF-401-NA)	R&D Systems, Minneapolis, MN, USA
IL-6 (AB-406-NA)	R&D Systems, Minneapolis, MN, USA
SKP1 (H-6; sc-5281)	Santa Cruz Biotechnology, Dallas, TX, USA
SKP1 (GTX106675)	GeneTex, Irvine, CA, USA
IκBα antibody (#9242)	Cell Signaling Technology, Beverly, MA, USA
phospho- NF-κB p65 (Ser536; #3033)	Cell Signaling Technology, Beverly, MA, USA
NF-κB p65 (D14E12; #8242)	Cell Signaling Technology, Beverly, MA, USA
β-actin (#4967)	Cell Signaling Technology, Beverly, MA, USA
Histone H1 (AE-4; sc-8030)	Santa Cruz Biotechnology, Dallas, TX, USA
LaminB1 (12987-1-AP)	ProteinTech, Rosemont, IL, USA
βTrCP (sc-390629)	Santa Cruz Biotechnology, Dallas, TX, USA
CUL-1 (sc-17775)	Santa Cruz Biotechnology, Dallas, TX, USA
RBX1 (sc-393640)	Santa Cruz Biotechnology, Dallas, TX, USA
HRP-conjugated anti-rabbit IgG (#7074)	Cell Signaling Technology, Beverly, MA, USA
HRP-conjugated anti-mouse IgG (#7076)	Cell Signaling Technology, Beverly, MA, USA
HRP-conjugated Rabbit Anti-Goat IgG (SA00001-4)	ProteinTech, Rosemont, IL, USA
Alexa Fluor 488-conjugated goat anti-rabbit IgG (A31627)	Invitrogen, Carlsbad, CA, USA
Alexa Fluor 488-conjugated goat anti-mouse IgG (A28175)	Invitrogen, Carlsbad, CA, USA

TNF-α: tumor necrosis factor-alpha; IL-1β: interleukin-1 beta; IL-6: interleukin-6; SKP1: S-phase kinase-associated protein 1; IκBα: nuclear factor of kappa light polypeptide gene enhancer in B-cells inhibitor, alpha; NF-κB: nuclear factor-kappa B; βTrCP: beta transducin repeat containing protein; CUL-1: cullin 1; RBX1: ring-box 1

Supplementary Fig. S1

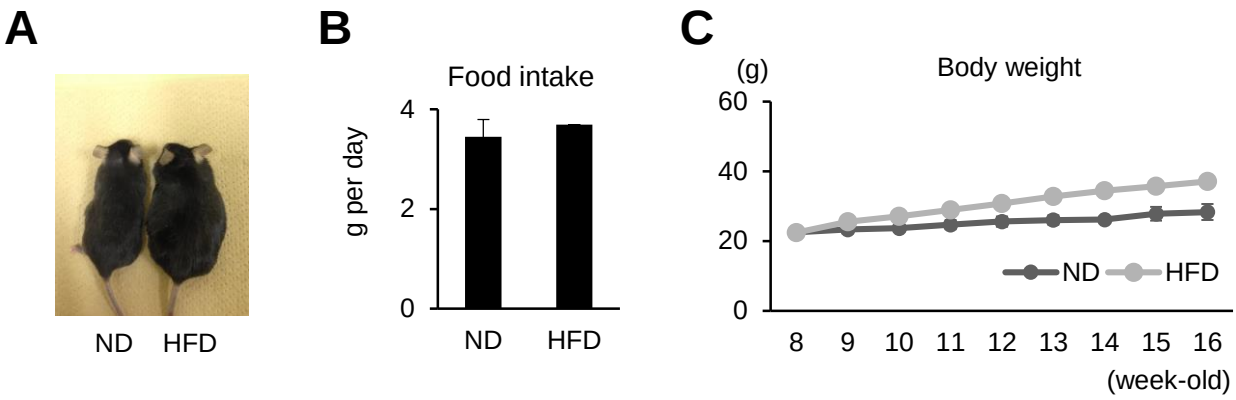

Supplementary Fig. S2

TNF-α (17 kDa)

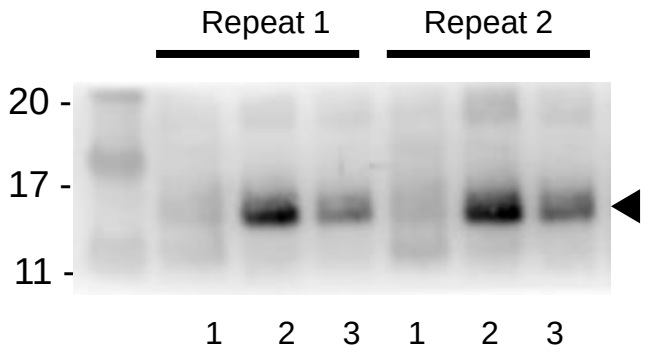

IL-1β (35 kDa)

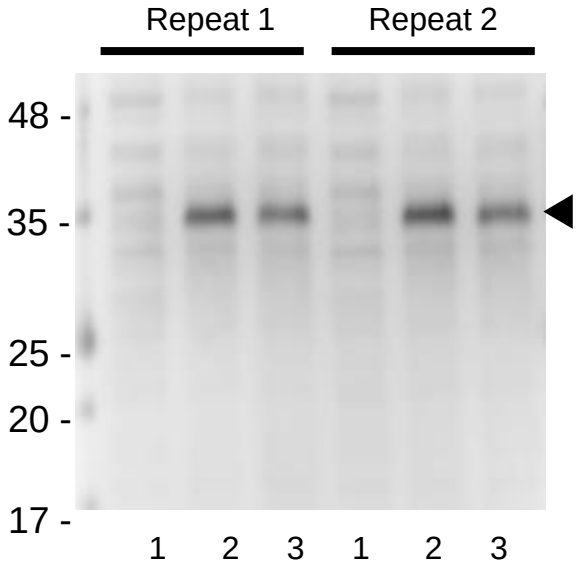

IL-6 (22–28 kDa)

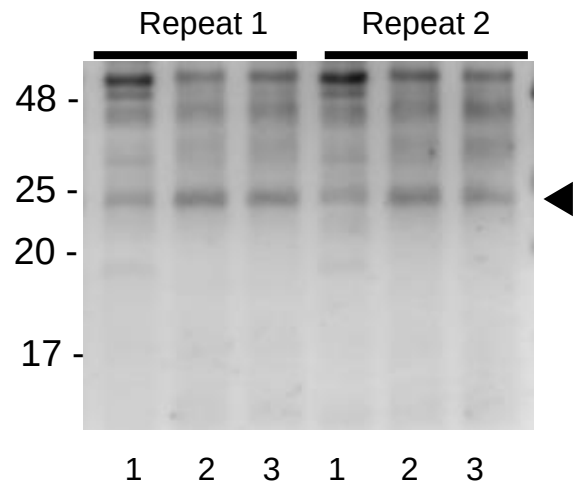

β-actin (45 kDa)

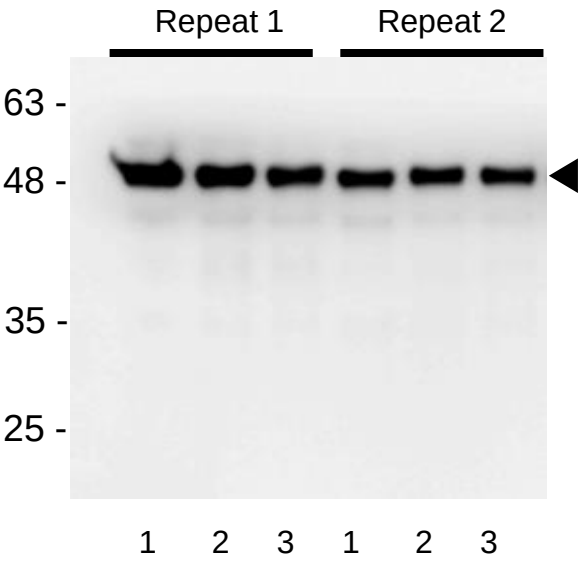

Supplementary Fig. S3

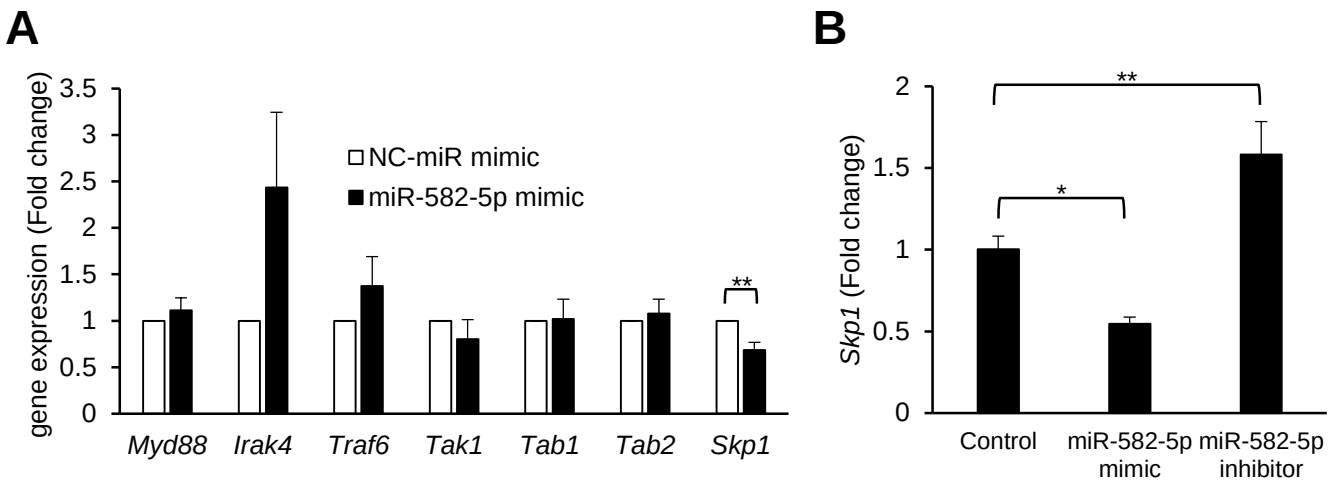

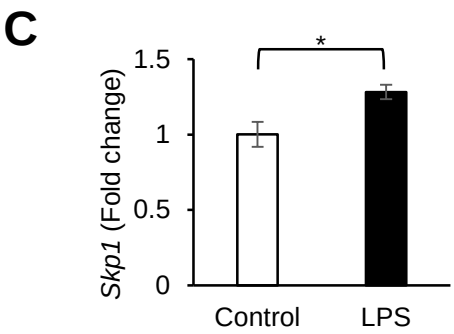

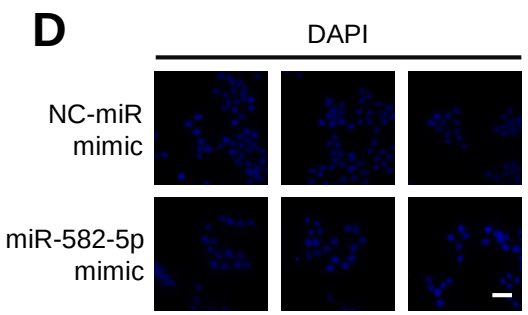

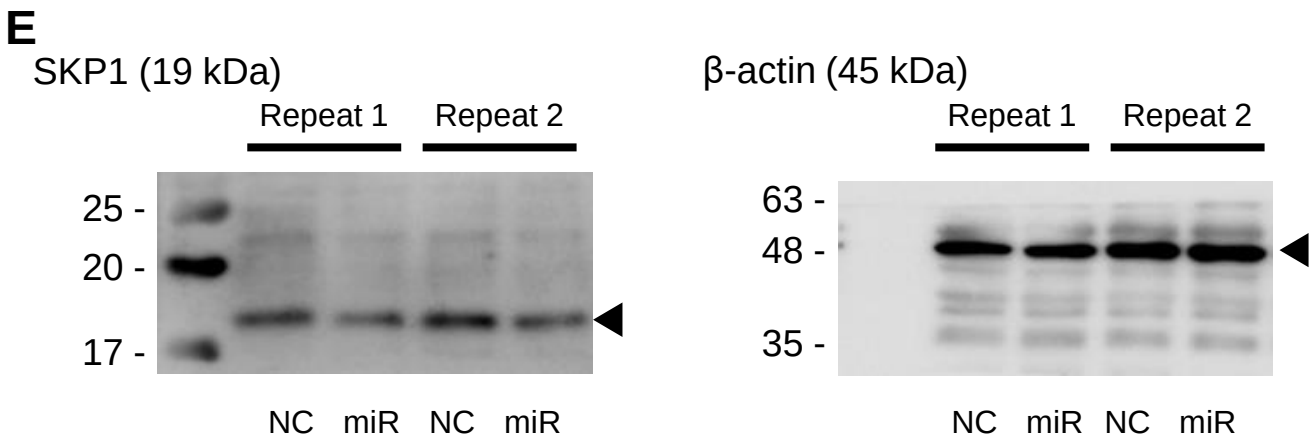

Supplementary Fig. S4

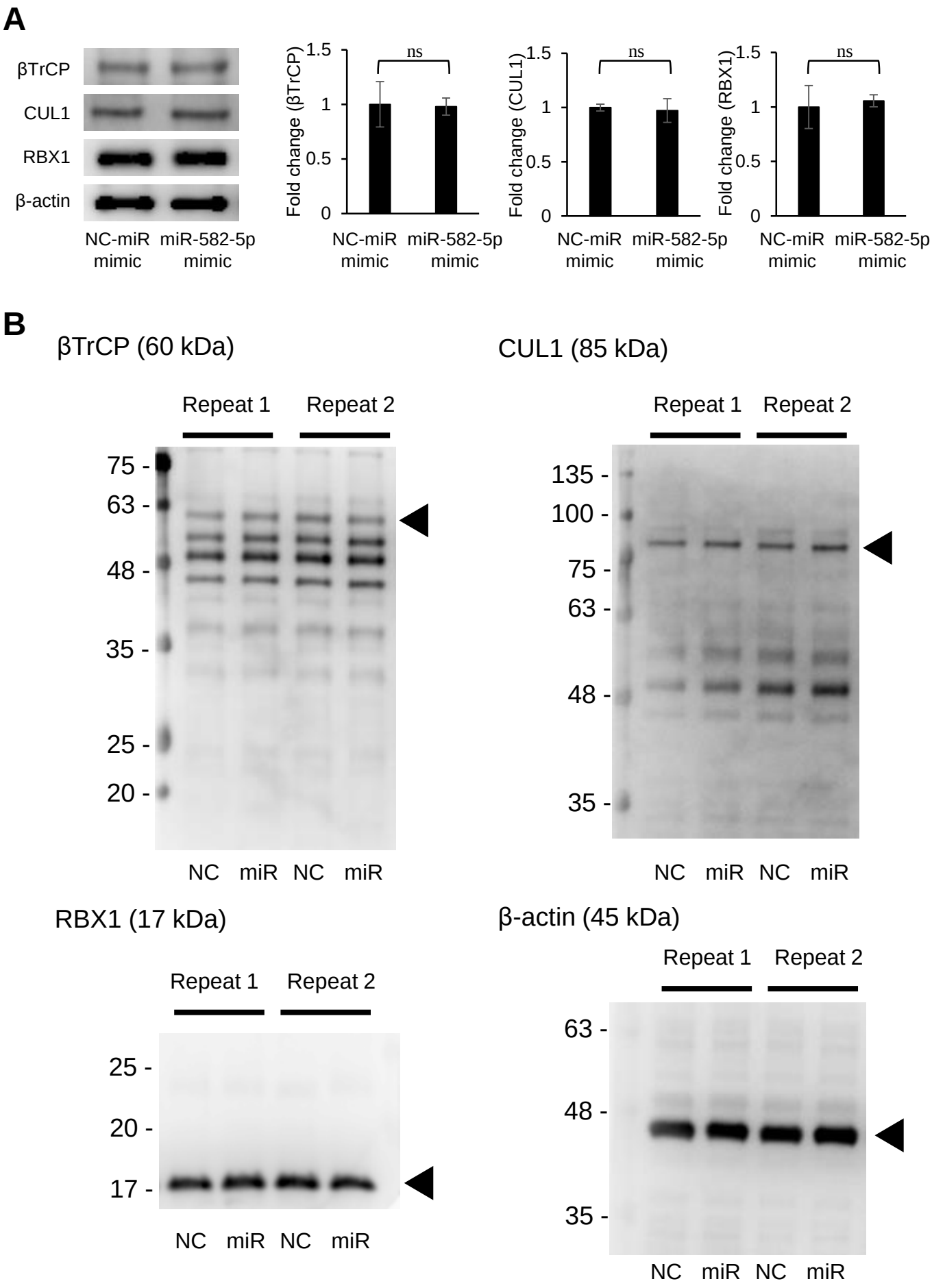

Supplementary Fig. S5

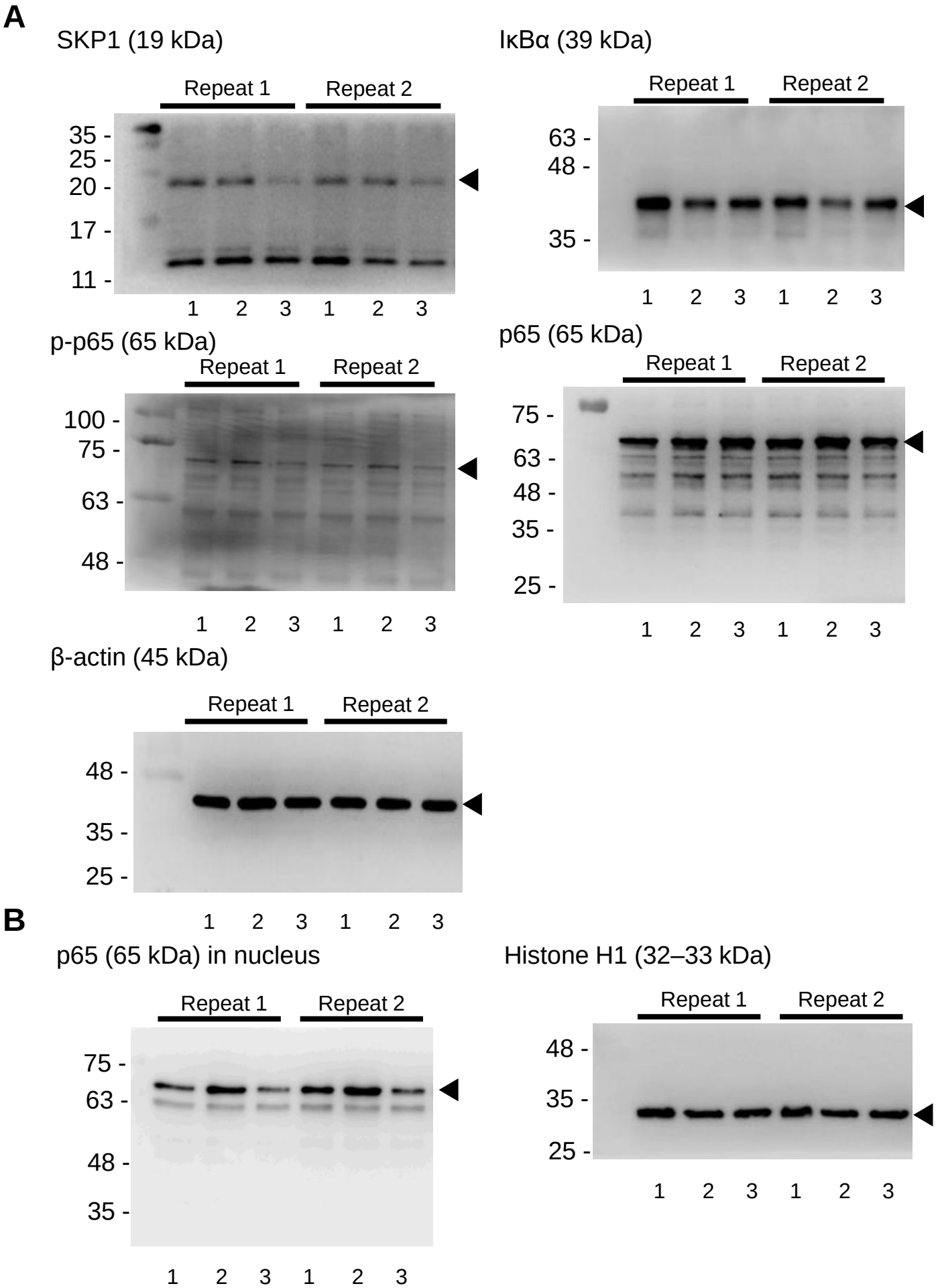

Supplementary Fig. S6

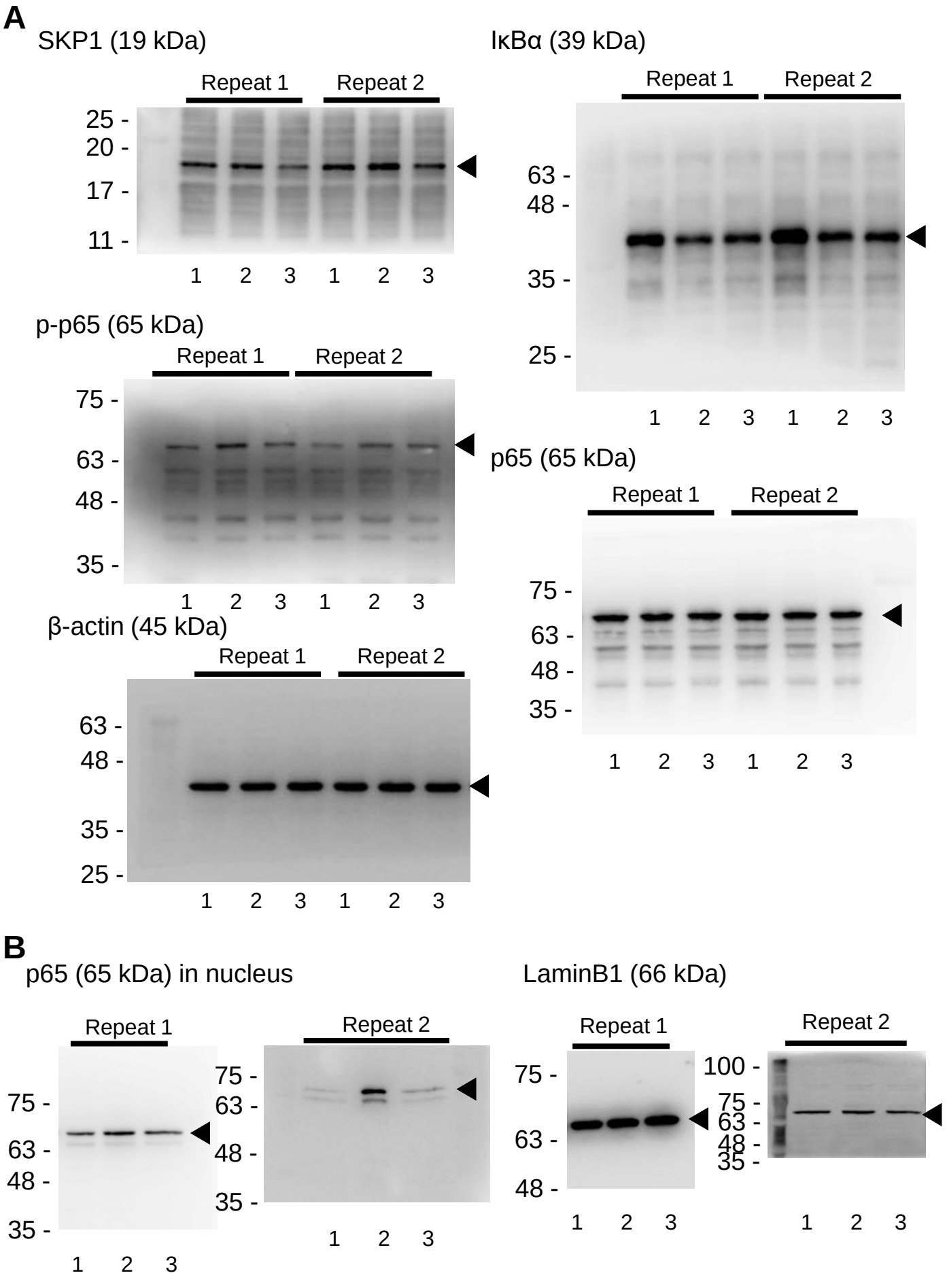

Supplementary Fig. S7

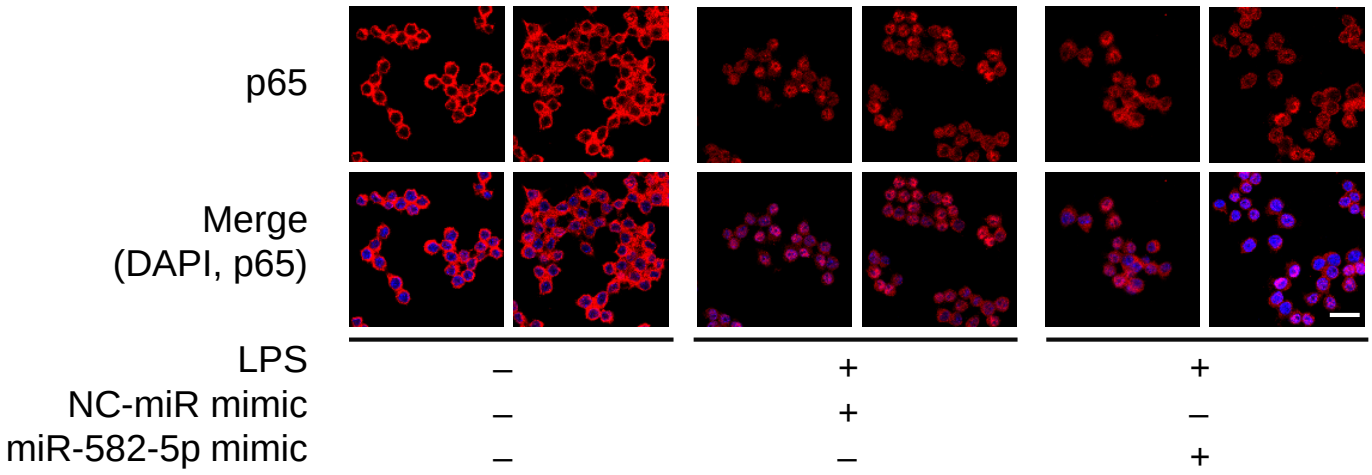

Supplementary Figure Legends

Supplementary Fig. S1. To study HFD-induced obesity, male C57BL/6J mice were fed with ND or HFD for 8 weeks until 16 weeks of age. (A) Representative photo of mice after 8 weeks of ND or HFD feeding. (B, C) Measurements of food intake (B) and body weight (C).

Supplementary Fig. S2. RAW264.7 cells were transfected with the control microRNA mimic (lane 2) or the miR-582-5p mimic (lane 3) for 24 h, followed by incubation with (lane 2 and 3) or without (lane 1) LPS for 4 h. The molecular weights of TNF-α, IL-1β, IL-6, and β-actin are 17 kDa, 35 kDa, 22–28 kDa, and 45 kDa, respectively. Molecular weight markers (in thousands) are shown on the left-hand side of each blot. Arrowheads represent the position of each immunoreactive band.

Supplementary Fig. S3. (A) RAW264.7 cells were transfected with the miR-582-5p mimic (20 nM) or its corresponding negative control microRNA mimic (NC-miR mimic, 20 nM) for 24 h. Then, mRNA was isolated and subjected to quantitative real-time PCR analysis. Bar graphs represent the mean ± SD (n = 3 for each group) relative to the NC-miR mimic transfected group. *Gapdh* was used as the internal reference gene. $^{**}p < 0.01$ represent significant differences between the indicated bars (Student's *t*-test). *Myd88*: myeloid differentiation primary response gene 88; *Irak4*: interleukin-1 receptor-associated kinase 4; *Traf6*: TNF receptor-associated factor 6; *Tak1*: mitogen-activated protein kinase kinase kinase 7; *Tab1*: TGF-beta activated kinase 1/MAP3K7 binding protein 1; *Tab2*: TGF-beta activated kinase 1/MAP3K7 binding protein 2; *Skp1*: S-phase kinase-associated protein 1. (B) RAW264.7 cells were transfected with the miR-582-5p mimic (20 nM) or the miR-582-5p inhibitor (20 nM) for 24 h. Then, mRNA was isolated and subjected to quantitative real-time PCR analysis. Bar graphs represent the mean ± SD (n = 3 for each group). *Gapdh* was used as the internal reference gene. $^{*}p < 0.05$, $^{**}p < 0.01$, represent significant differences between the indicated bars (Tukey-Kramer's HSD-test). (C) RAW264.7 cells were incubated with (LPS) or without (Control) LPS for 2 h. Then, mRNA was isolated, and

Skp1 mRNA expression was measured using quantitative real-time PCR analysis. We repeated this experiment thrice. *Gapdh* was used as the internal reference gene. Bar graphs represent the mean ± SD (n = 3 for each group). *$p < 0.05$ represent significant differences between the indicated bars (Student's *t*-test). (D) RAW264.7 cells were transfected with the miR-582-5p mimic (20 nM) or the negative control microRNA mimic (NC-miR mimic, 20 nM) for 24 h. The nuclei were counterstained with DAPI (blue). Scale bar = 20 μm. (E) Two other data sets (Repeat 1 and 2) of Fig. 3D are shown. The molecular weights of SKP1 and β-actin are 19 kDa and 45 kDa, respectively. NC and miR represent the data from cells transfected with the negative control microRNA mimic and miR-582-5p mimic, respectively. Molecular weight markers (in thousands) are shown on the left-hand side of each blot. Arrowheads represent the position of each immunoreactive band.

Supplementary Fig. S4. (A) RAW264.7 cells were transfected with either the miR-582-5p mimic (20 nM) or its corresponding negative control microRNA mimic (NC-miR mimic, 20 nM) for 24 h. The protein levels of βTrCP, CUL1, and RBX1 were examined using western blotting. A set of representative blots from three independent experiments are shown. β-actin was used as the loading control. Bar graphs represent the mean ± SD (n = 3 for each group). ns, not significant (Student's *t*-test). (B) We repeated the above experiment thrice. The other two data sets are shown as repeat 1 and 2 in (B). Molecular weight markers (in thousands) are shown on the left-hand side of each blot. The molecular weights of βTrCP, CUL1, RBX1, and β-actin are 60 kDa, 85 kDa, 17 kDa, and 45 kDa, respectively. Arrowheads represent the position of each immunoreactive band. NC and miR represent the data from cells transfected with the negative control microRNA mimic and miR-582-5p mimic, respectively. βTrCP: beta transducin repeat-containing protein; CUL1: cullin 1; RBX1: ring-box 1.

Supplementary Fig. S5. (A, B) RAW264.7 cells were transfected with si-control (lane 2) or si-*Skp1* (lane 3) for 24 h, followed by incubation with (lane 2, 3) or without (lane 1) LPS for 90 min;

cell lysates (A) or nuclear fraction (B) were analyzed. We repeated this experiment thrice; one set of data is shown in Fig. 4B and C, and the other two other original images (Repeat 1 and 2) are shown (A, B). The molecular weights of SKP1, IκBα, p65 (p-p65), β-actin, and histone H1 are 19 kDa, 39 kDa, 65 kDa, 45 kDa, and 32–33 kDa, respectively. Molecular weight markers (in thousands) are shown on the left-hand side of each blot. Arrowheads represent the position of each immunoreactive band.

Supplementary Fig. S6. (A, B) RAW264.7 cells were transfected with the control microRNA mimic (lane 2) or the miR-582-5p mimic (lane 3) for 24 h, followed by the incubation with (lane 2, 3) or without (lane 1) LPS for 90 min; cell lysates (A) or nuclear fraction (B) were analyzed. We repeated these experiments thrice; one set of data is shown in Fig. 4D and E, and the other two original images (Repeat 1 and 2) are shown (A, B). The molecular weights of SKP1, IκBα, p65 (p-p65), β-actin, and lamin B1 are 19 kDa, 39 kDa, 65 kDa, 45 kDa, and 66 kDa, respectively. Molecular weight markers (in thousands) are shown on the left-hand side of each blot. Arrowheads represent the position of each immunoreactive band.

Supplementary Fig. S7. RAW264.7 cells were transfected with the miR-582-5p mimic (20 nM) or negative control microRNA mimic (NC-miR mimic, 20 nM) for 24 h and then incubated with or without LPS for 90 min. The cells were analyzed through immunofluorescence staining using an anti-p65 antibody. Two sets of images of p65 immunofluorescence staining (red) are shown. The nuclei were counterstained with DAPI (blue). Scale bar = 20 μm.